

3. M. Yoshizawa, M. Tamura, M. Fujita, *Science* **312**, 251–254 (2006).
4. J. Kang, J. Rebek Jr., *Nature* **385**, 50–52 (1997).
5. Q. Zhang, K. Tiefenbacher, *Nat. Chem.* **7**, 197–202 (2015).
6. W. M. Hart-Cooper, K. N. Clary, F. D. Toste, R. G. Bergman, K. N. Raymond, *J. Am. Chem. Soc.* **134**, 17873–17876 (2012).
7. C. J. Hastings, M. D. Pluth, R. G. Bergman, K. N. Raymond, *J. Am. Chem. Soc.* **132**, 6938–6940 (2010).
8. M. L. Merlau, M. del Pilar Mejia, S. T. Nguyen, J. T. Hupp, *Angew. Chem. Int. Ed.* **40**, 4239–4242 (2001).
9. J. Meeuwissen, J. N. H. Reek, *Nat. Chem.* **2**, 615–621 (2010).
10. J. F. Hartwig, in *Organotransition Metal Chemistry: From Bonding to Catalysis* (University Science Books, Mill Valley, CA, 2010), pp. 321–348, 877–883.
11. A. L. Liberman-Martin, R. G. Bergman, T. D. Tilley, *J. Am. Chem. Soc.* **135**, 9612–9615 (2013).
12. A. Hazari, J. A. Labinger, J. E. Bercaw, *Angew. Chem. Int. Ed.* **51**, 8268–8271 (2012).
13. Q. Shen, J. F. Hartwig, *J. Am. Chem. Soc.* **129**, 7734–7735 (2007).
14. T. Yamamoto, A. Yamamoto, S. Ikeda, *J. Am. Chem. Soc.* **93**, 3350–3359 (1971).
15. W. Lau, J. C. Huffman, J. K. Kochi, *Organometallics* **1**, 155–169 (1982).
16. V. Lavallo, R. H. Grubbs, *Science* **326**, 559–562 (2009).
17. S. Takemoto, V. V. Grushin, *J. Am. Chem. Soc.* **135**, 16837–16840 (2013).
18. J. P. Collman, R. G. Finke, J. N. Cawse, J. I. Brauman, *J. Am. Chem. Soc.* **100**, 4766–4772 (1978).
19. R. Jana, T. P. Pathak, M. S. Sigman, *Chem. Rev.* **111**, 1417–1492 (2011).
20. D. Fiedler, R. G. Bergman, K. N. Raymond, *Angew. Chem. Int. Ed.* **45**, 745–748 (2006).
21. Z. J. Wang, C. J. Brown, R. G. Bergman, K. N. Raymond, F. D. Toste, *J. Am. Chem. Soc.* **133**, 7358–7360 (2011).
22. C. J. Brown, F. D. Toste, R. G. Bergman, K. N. Raymond, *Chem. Rev.* **115**, 3012–3035 (2015).
23. S. Komiya, J. K. Kochi, *J. Am. Chem. Soc.* **98**, 7599–7607 (1976).
24. P. Lawrence Kuch, R. Stuart Tobias, *J. Organomet. Chem.* **122**, 429–446 (1976).
25. O. Schuster, H. Schmidbauer, *Z. Naturforsch. B* **61**, 1–5 (2006).
26. K. I. Goldberg, J. Y. Yan, E. L. Winter, *J. Am. Chem. Soc.* **116**, 1573–1574 (1994).
27. **2-Br** was employed rather than **2** because it was expected to show a higher affinity for the interior of **1**, on the basis of previous observations in similar systems (19). The calculated value for  $k_{cat}$  is necessarily identical for **2** and **2-Br** because of the mechanistic convergence in the encapsulated intermediate.
28. D. G. Blackmond, *Angew. Chem. Int. Ed.* **44**, 4302–4320 (2005).
29. R. B. Silverman, in *The Organic Chemistry of Enzyme-Catalyzed Reactions* (Academic Press, San Diego, CA, 2002), p. 15.
30. A. E. Allen, D. W. C. Macmillan, *Chem. Sci.* **2012**, 633–658 (2012).
31. C. Zhao *et al.*, *J. Am. Chem. Soc.* **135**, 18802–18805 (2013).
32. C. C. C. Johansson Seechurn, M. O. Kitching, T. J. Colacot, V. Snieckus, *Angew. Chem. Int. Ed.* **51**, 5062–5085 (2012).

## ACKNOWLEDGMENTS

This research was supported by the Director, Office of Science, Office of Basic Energy Sciences and the Division of Chemical Sciences, Geosciences, and Biosciences of the U.S. Department of Energy at Lawrence Berkeley National Laboratory (grant DE-AC02-05CH11231) and NIH National Institute of General Medical Sciences (grant R01 GM073932). D.M.K. was supported by an NSF Graduate Research Fellowship Program (GRFP) (grant DGE 1106400), and M.D.L. was supported by the ARCS Foundation and an NSF GRFP. We thank J. N. Brantley and M. S. Winston for helpful discussions and C. G. Canlas for assistance with NMR experiments.

## SUPPLEMENTARY MATERIALS

www.sciencemag.org/content/350/6265/1235/suppl/DC1  
Materials and Methods  
Figs. S1 to S42  
References

25 August 2015; accepted 23 October 2015  
10.1126/science.aad3087

## SOLAR PHYSICS

# Particle acceleration by a solar flare termination shock

Bin Chen,<sup>1\*</sup> Timothy S. Bastian,<sup>2</sup> Chengcai Shen,<sup>1</sup> Dale E. Gary,<sup>3</sup>  
Säm Krucker,<sup>4,5</sup> Lindsay Glesener<sup>4,6</sup>

Solar flares—the most powerful explosions in the solar system—are also efficient particle accelerators, capable of energizing a large number of charged particles to relativistic speeds. A termination shock is often invoked in the standard model of solar flares as a possible driver for particle acceleration, yet its existence and role have remained controversial. We present observations of a solar flare termination shock and trace its morphology and dynamics using high-cadence radio imaging spectroscopy. We show that a disruption of the shock coincides with an abrupt reduction of the energetic electron population. The observed properties of the shock are well reproduced by simulations. These results strongly suggest that a termination shock is responsible, at least in part, for accelerating energetic electrons in solar flares.

The acceleration of charged particles to high energies occurs throughout the universe. Understanding the physical mechanisms is a fundamental topic in many space, astrophysical, and laboratory contexts that involve magnetized plasma (1). For solar flares and the often-associated coronal mass ejections (CMEs), it is generally accepted that fast mag-

netic reconnection—the sudden reconfiguration of the magnetic field topology and the associated magnetic energy release—serves as the central engine driving these powerful explosions. However, the mechanism for converting the released magnetic energy into the kinetic energy in accelerated particles has remained uncertain (2, 3). Competing mechanisms include acceleration by the reconnection current sheet, turbulence, and shocks (2–5).

Of possible interest in this regard is the termination shock (TS), produced by super-magnetosonic reconnection outflows impinging upon dense, closed magnetic loops in a cusp-shaped reconnection geometry (6). Although often invoked in the standard picture of solar flares (7, 8) and predicted in numerical simulations (6, 9–11), its presence has yet to be firmly established observationally and, because of the paucity of direct observation-

al evidence, its role as a possible particle accelerator has received limited attention (2, 3). Previous reports of coronal hard x-ray (HXR) sources in some flares have shown convincing evidence of the presence of accelerated electrons at or above the top of flare loops (referred to as the “loop-top” hereafter, or LT) (7, 12), where a TS is presumably located. The often-cited observational evidence for a solar flare TS has been certain radio sources showing spectroscopic features similar to solar type II radio bursts (radio emission associated with propagating shocks in the outer corona), but with small drifts in their emission frequency as a function of time, which implies a standing shock wave (13–17). However, because of the limited spectral imaging capabilities of the previous observations, none of these have shown direct signatures of the TS in terms of its characteristic morphology and dynamics, as well as a clear relation to the reconnection outflows, so that a definitive association with a TS could be demonstrated.

We present observations of a TS in an eruptive solar flare using the Karl G. Jansky Very Large Array (VLA). This eruption occurred close to the east limb of the Sun on 3 March 2012 (Fig. 1A), producing a fast white light CME [ $\sim 1000 \text{ km s}^{-1}$ ; observed by the Large Angle and Spectrometric Coronagraph Experiment (LASCO)] and a C1.9-class long-duration flare (18). It displayed a cusp-shaped reconnection geometry typical of the standard scenario of eruptive solar flares (7, 8), in which the eruption outward into the upper corona stretches magnetic field lines behind it and induces a vertical current sheet, where magnetic reconnection occurs. The reconnected field lines below the reconnection site are pulled downward by magnetic tension to form an arcade of magnetic loops anchored at the solar surface. The arcade of reconnected loops subsequently fills with hot plasma and becomes bright in extreme ultraviolet (EUV) and soft x-ray (SXR) wavelengths. For this event, the eruption, the current-sheet-like structure, and the

<sup>1</sup>Harvard-Smithsonian Center for Astrophysics, 60 Garden Street, Cambridge, MA 02138, USA. <sup>2</sup>National Radio Astronomy Observatory, 520 Edgemont Road, Charlottesville, VA 22903, USA. <sup>3</sup>New Jersey Institute of Technology, 323 Martin Luther King Boulevard, Newark, NJ 07102, USA. <sup>4</sup>University of California, Berkeley, 7 Gauss Way, Berkeley, CA 94720, USA. <sup>5</sup>University of Applied Sciences and Arts Northwestern Switzerland, Bahnhofstrasse 6, 5210 Windisch, Switzerland. <sup>6</sup>University of Minnesota, Twin Cities, 116 Church Street SE, Minneapolis, MN 55455, USA.  
\*Corresponding author. E-mail: bin.chen@njit.edu

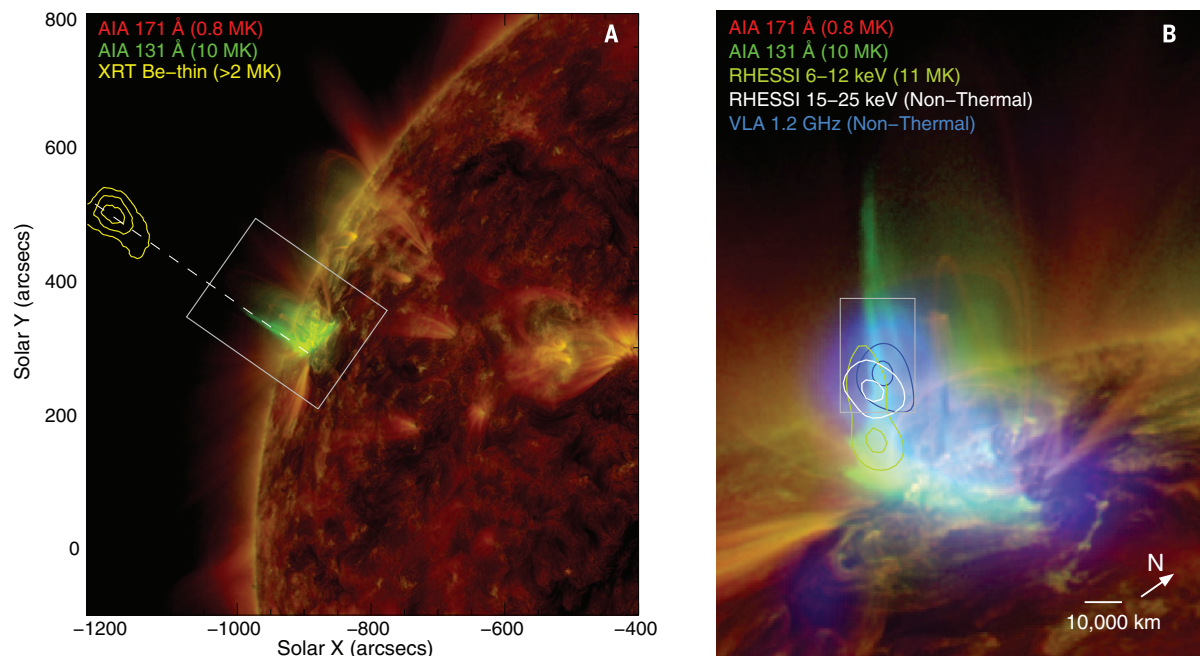


**Fig. 1. Solar flare seen in multiple wavelengths.** (A) The eruptive flare observed in EUV and x-ray wavelengths by the Atmospheric Imaging Assembly (AIA) 171 Å (red), X-Ray Telescope (XRT; aboard the Hinode satellite) Be-thin (yellow contours, showing the eruption), and AIA 131 Å (green, showing the newly reconnected flare loops) passbands, which are respectively sensitive to plasma temperatures of 0.8, >2, and 10 MK. (B) Closer view of the flaring region [box in (A), rotated clockwise to an upright orientation]. A radio source (blue; at 1.2 GHz) is observed at the top of hot flaring loops (~10 MK), which is nearly cospatial with a nonthermal HXR source (white contours; at 15 to 25 keV) seen by the Reuven Ramaty High Energy Solar Spectroscopic Imager (RHESSI).

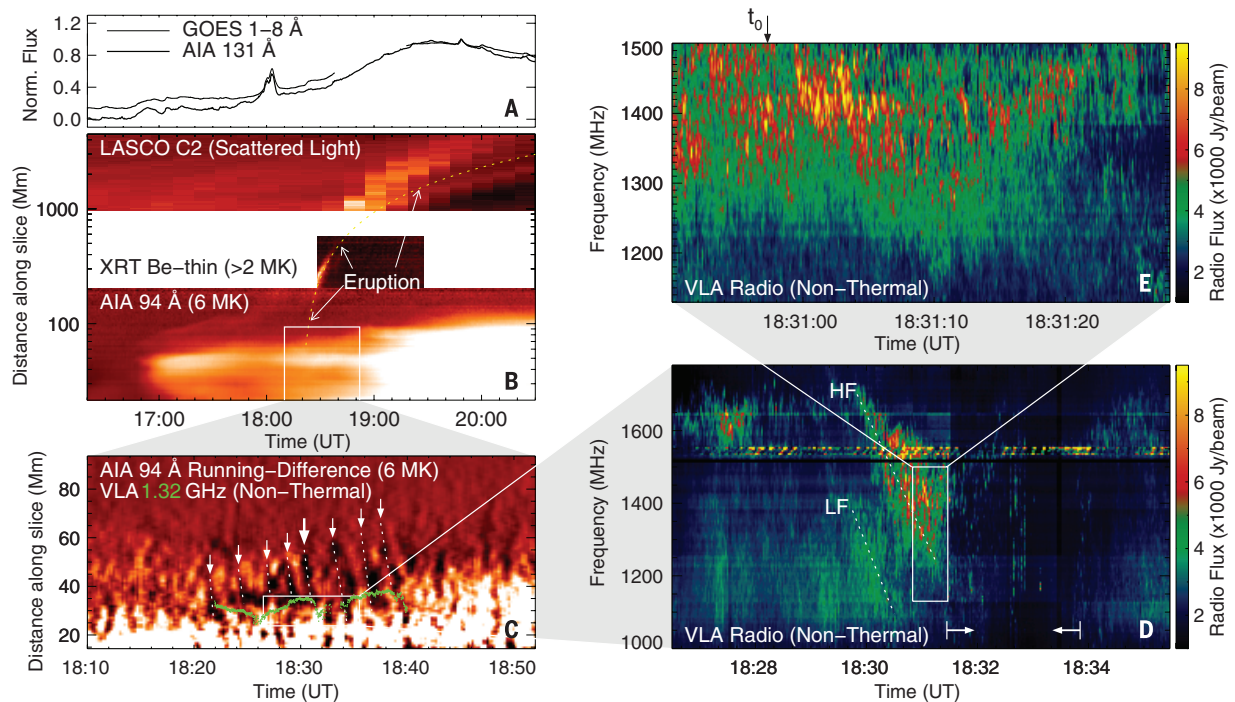


**Fig. 2. Radio emission at the front of fast reconnection outflows.** (A) EUV and x-ray light curves showing the time history of the radiating hot plasmas ( $\geq 10$  MK) of the flare event. The TS is observed during the flare rise phase. (B) Time-distance plot of the EUV, x-ray, and white light intensities, showing the evolution of the eruption and the underlying flare loops, obtained at the slice in Fig. 1A (dashed line). (C) Running-difference space-time plot of EUV 94 Å zoomed in to the LT region. A series of fast PDs are visible as features with a negative slope (indicated by small white arrows; the PD

associated with the TS disruption in Fig. 3 is marked by a large white arrow). The stochastic spike bursts are located near the endpoint of these PDs (green dots). Its spectrotemporal intensity variation is shown in the spatially resolved, or “vector” dynamic spectrum of (D) and (E), manifesting as many short-lived, narrow-frequency-bandwidth radio bursts. Two dotted lines in (D) mark the split-band feature (HF and LF denote the high- and low-frequency branch, respectively). A pair of arrows brackets a period when the TS experiences a major disruption, starting from 18:31:27 UT (start time  $t_0$ ).

cusp-shaped magnetic loops are all clearly visible in EUV and SXR passbands that are sensitive to plasma hotter than  $\sim 2$  MK (Fig. 1A). A non-thermal HXR source appears at the LT during the rise phase of the flare, indicating the presence of accelerated electrons at this location (Fig. 1B).

VLA images at 1 to 1.8 GHz show a localized radio source nearly cospatial with the HXR LT source, in addition to two other sources located near the conjugate magnetic footpoints (FPs) of the flaring loops (Fig. 1B and fig. S1). The VLA's simultaneous high spectral and temporal resolution (1 MHz and 50 ms, respectively, enabling high-cadence radio imaging spectroscopy) reveals the highly dynamic and fragmented nature of this LT radio source. It consists of thousands of short-lived ( $< 50$  ms) and narrow-frequency bandwidth (with spectral width  $\delta\nu/\nu \approx 2\%$ ) brightenings (Fig. 2, D and E) (19). These observations strongly imply that many short-lived emission events, which we term stochastic radio spikes, are occurring at the LT, which, as we will demonstrate, are associated with a dynamic TS.

Difference imaging in the EUV 94 Å passband of the Atmospheric Imaging Assembly (AIA)

aboard the Solar Dynamics Observatory (20) reveals that many recurring plasma downflows (PDs) stream rapidly (at  $\sim 550$  km/s in projection) along the current sheet from the reconnection site downward to the flaring, reconnected loops. They end near the same location as the LT radio and HXR sources (Fig. 2C). These fast PDs are thought to be associated with magnetic structures embedded in reconnection outflows, probably in the form of rapidly contracting magnetic loops (22). The relative locations of the PDs and the radio/HXR LT sources agree very well with the scenario in which a TS forms at the ending fronts of fast reconnection outflows and drives particle acceleration.

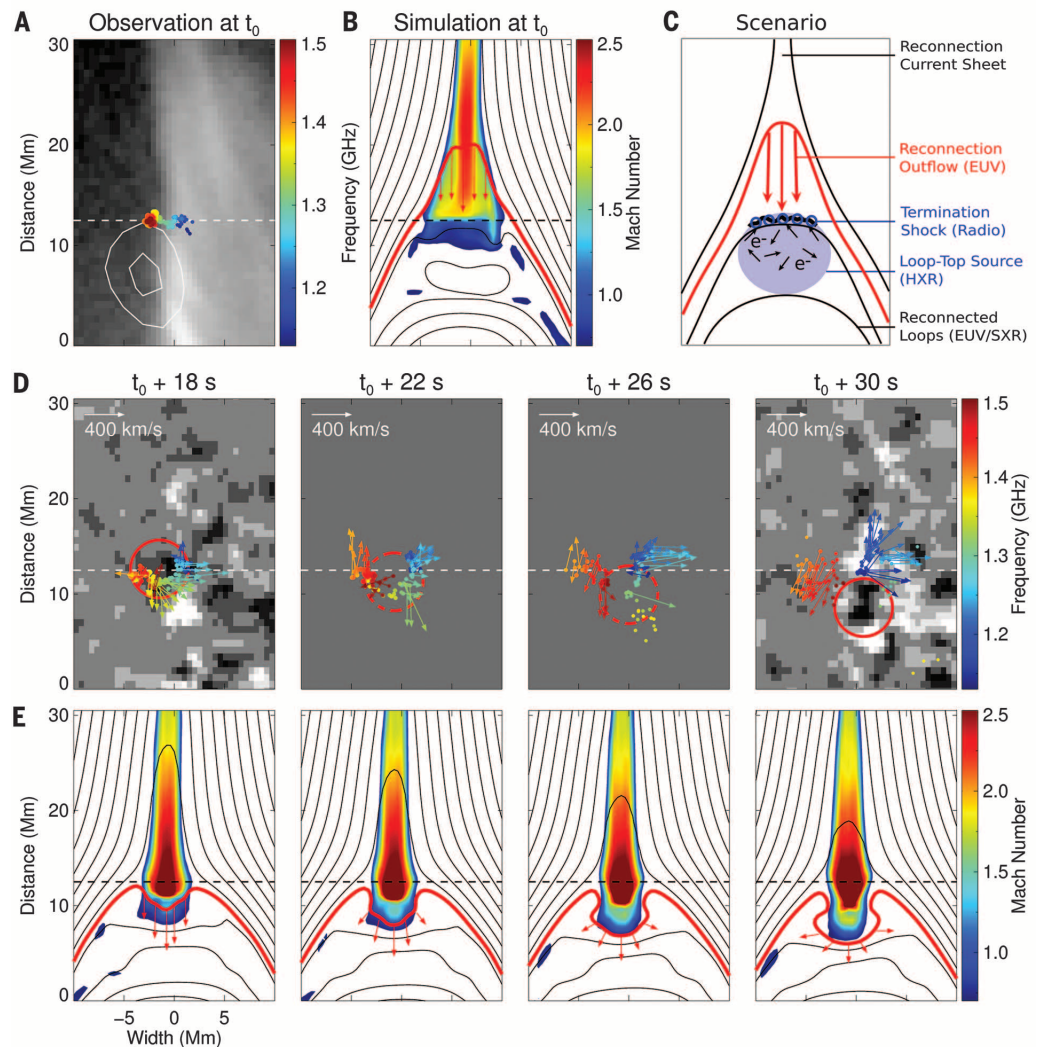
The most direct observational evidence of the TS comes from the instantaneous spatial distribution of the myriad radio spikes at different frequencies, which forms a narrow surface at the LT region (Fig. 3A). The location and morphology of this surface closely resemble those of a TS, as predicted in numerical simulations when viewed edge-on [(6, 9–11); see also Fig. 3B]. The coronal HXR source is located slightly below this surface and evolves coherently with it (Fig. 3A and fig. S4), suggesting that this is nonthermal

emission from accelerated electrons confined in the shock downstream region, possibly due to strong pitch-angle scattering and/or magnetic trapping in the turbulent environment (21). The TS is probably a weak quasi-perpendicular fast-mode shock, based on multiple lines of evidence (19). A Mach number of  $M \approx 1.5$  can be inferred based on the interpretation of the split-band feature seen in the radio dynamic spectrum [marked HF (high-frequency) and LF (low-frequency) in Fig. 2D (19)].

The TS front, as outlined by the radio spikes, reacts dynamically to the arrival of the fast PDs. Some PDs cause only partial disruption of the TS front, and the shock is quickly restored to its original state. Some other PDs, however, cause a major disruption of the TS. This process starts with the quasi-flat TS front being first driven concave-downward by a PD, followed by a break-up of the TS (Fig. 3D and fig. S4). To understand the dynamic nature of the TS, we used a magnetohydrodynamics (MHD) model to simulate magnetic reconnection in a standard flare geometry based on physical values constrained by the observations (19). The model shows that reconnection outflows with super-magnetosonic speeds

### Fig. 3. Observation and simulation of the dynamic TS. (A)

A closer view of the LT region (white box in Fig. 1B) at 18:30:57 UT ( $t_0$  in Fig. 2E). The TS appears as a dynamic surface delineated by the many unresolved radio sources, each of which corresponds to a radio spike in the dynamic spectrum at a given time and frequency (colored dots indicate their centroid location). White contours show the coronal HXR source at 15 to 25 keV. The grayscale background is the AIA 94 Å intensity. (B) The TS is seen in the MHD simulation as a sharp layer of velocity discontinuity at the LT. The fast-mode magnetosonic Mach number is shown in color, overlaid with magnetic field lines. (C) Physical scenario of emission processes near the TS. Radio spikes are emitted as accelerated electrons impinge on density fluctuations at the shock (blue circles). These electrons also produce a HXR source in the shock downstream region (blue shadowed region). (D and E) Observation and simulation of the TS disruption. A fast PD identified in the AIA 94 Å running-difference images (red circles) arrives at the TS at  $\sim 18:31:15$  UT ( $t_0 + 18$ s) and disrupts the shock, which appears in the simulation as a rapidly contracting magnetic loop (red curve). Arrows show the velocity vectors.



can produce a TS in the LT region, and the observed morphology and dynamics of the TS are well reproduced by the simulations (Fig. 3, B and E, and movie S1). In the simulations, the observed PDs correspond to magnetic structures formed because of instabilities in the reconnection current sheet, which may facilitate the efficiency of the magnetic energy release that powers solar flares (22).

During the largest disruption of the TS, the intensities of all of the three widely separated radio sources decrease simultaneously. The HXR flux above 15 keV is also abruptly reduced, whereas the SXR flux (<12 keV) is largely unaffected, which is consistent with a temporarily softened x-ray photon spectrum (Fig. 4). Both phenomena suggest a temporary decrease of the number of energetic electrons. By fitting the observed x-ray spectrum using an isothermal plasma plus a nonthermal electron distribution with a power-law form, we confirmed that energetic electrons were much less abundant during the shock destruction: the total number of >18 keV electrons was reduced by ~62% (19). This is strong evidence that the TS plays a key role in accelerating the energetic electrons.

An important question is what emission mechanism is responsible for the multitudes of narrow-band stochastic radio spikes at the TS. An attractive possibility is linear mode conversion of Langmuir waves on small-scale density fluctuations (23, 24), a mechanism that has been explored in the context of radio bursts in the solar corona, in Earth's foreshock region, and near the heliospheric TS (24–26). This mechanism requires both a source of Langmuir waves and the presence of small-scale density fluctuations. We suggest that electrons are accelerated in the turbulent plasma environment at the TS (5, 16, 27, 28), an assumption supported by the HXR source at the LT (Fig. 3C). These accelerated electrons are unstable to the production of Langmuir waves, which impinge on the small-scale density fluctuations associated with the turbulent medium and convert to electromagnetic waves near the local plasma frequency  $\nu_{pe} = (e^2 n_e / \pi m_e)^{1/2} \approx 8980 \sqrt{n_e}$  Hz, where  $n_e$  is the electron density (23, 24). The frequency range of 1 to 1.8 GHz over which the spike bursts appear then implies a density range of  $n_e \approx 1.2 \times 10^{10}$  to  $4 \times 10^{10} \text{ cm}^{-3}$ , which is consistent with that from the x-ray spectral analysis (19). The level of the density fluctuations  $\delta n_e / n_e$  is

related to the observed spike bandwidths as  $\delta n_e / n_e \approx 2\delta\nu / \nu$ , which is relatively small (4%). The spatial scales of the density fluctuations are also small, a few hundred kilometers at the maximum (19).

A major theoretical concern regarding electron acceleration by a fast-mode quasi-perpendicular shock (as for the case of a TS) has been the injection problem: Electrons need to cross the shock front multiple times and/or be pre-accelerated to suprathermal energies in order to gain energy efficiently (2, 3, 27). Our observations show strong evidence for the existence of many small-scale low-amplitude fluctuations at the TS front, which may serve as scattering agents that cause repeated passage of the electrons across the shock (5, 27–30). In addition, the nonthermal electron population is reduced but not eliminated during the TS disruption (Fig. 4 and fig. S5), which implies that electrons may have been pre-accelerated before they reach the shock, possibly at or near the reconnection site (2–4, 12). Both signatures may contribute to resolving the injection problem.

By confirming the existence of the previously controversial solar flare TS and providing strong evidence for it being a particle accelerator, we have obtained new insights into the long-standing problem of particle acceleration in solar flares.

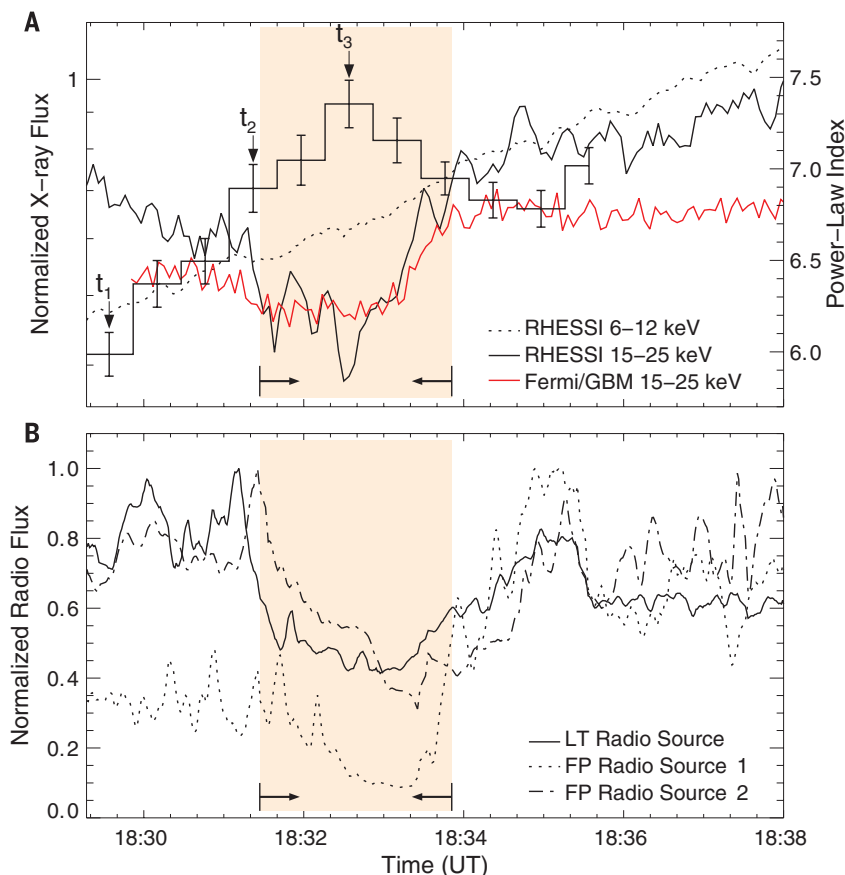


**Fig. 4. Reduction of x-ray and radio flux during shock disruption.** (A) Temporal evolution of total x-ray photon counts (curves) and power-law index of the x-ray photon spectrum (histogram). Examples of the observed and fitted x-ray spectra are shown in fig. S5 for selected times before and during the shock disruption (marked as  $t_1$ ,  $t_2$ , and  $t_3$ ). (B) Evolution of the spatially resolved radio flux of the LT source and the two FP sources, showing a co-temporal radio flux reduction (see also fig. S1C). Arrows bracket a period when the TS experiences a major disruption starting from 18:31:27 UT (or  $t_0 + 30$ s, corresponding to the last panel of Fig. 3D).

#### REFERENCES AND NOTES

1. Y. Matsumoto, T. Amano, T. N. Kato, M. Hoshino, *Science* **347**, 974–978 (2015).
2. J. A. Miller *et al.*, *J. Geophys. Res.* **102**, 14631–14660 (1997).
3. V. V. Zharkova *et al.*, *Space Sci. Rev.* **159**, 357–420 (2011).
4. J. F. Drake, M. Swisdak, H. Che, M. A. Shay, *Nature* **443**, 553–556 (2006).
5. S. Tsuneta, T. Naito, *Astrophys. J.* **495**, L67–L70 (1998).
6. T. G. Forbes, *Astrophys. J.* **305**, 553–563 (1986).
7. S. Masuda, T. Kosugi, H. Hara, S. Tsuneta, Y. Ogawara, *Nature* **371**, 495–497 (1994).
8. K. Shibata *et al.*, *Astrophys. J.* **451**, L83 (1995).
9. T. Yokoyama, K. Shibata, *Astrophys. J.* **494**, L113–L116 (1998).
10. J. C. Workman, E. G. Blackman, C. Ren, *Phys. Plasmas* **18**, 092902 (2011).
11. S. Takasao, T. Matsumoto, N. Nakamura, K. Shibata, *Astrophys. J.* **805**, 135 (2015).
12. W. Liu, Q. Chen, V. Petrosian, *Astrophys. J.* **767**, 168 (2013).
13. H. Aurass, B. Vršnak, G. Mann, *Astron. Astrophys.* **384**, 273–281 (2002).
14. H. Aurass, G. Mann, *Astrophys. J.* **615**, 526–530 (2004).
15. G. Mann, A. Warmuth, H. Aurass, *Astron. Astrophys.* **494**, 669–675 (2009).
16. A. Warmuth, G. Mann, H. Aurass, *Astron. Astrophys.* **494**, 677–691 (2009).
17. H. Aurass, G. Holman, S. Braune, G. Mann, P. Zlobec, *Astron. Astrophys.* **555**, A40 (2013).
18. B. Chen, T. S. Bastian, D. E. Gary, *Astrophys. J.* **794**, 149 (2014).
19. Materials and methods are available as supplementary materials on Science Online.
20. J. R. Lemen *et al.*, *Sol. Phys.* **275**, 17–40 (2012).
21. P. J. A. Simões, E. P. Kontar, *Astron. Astrophys.* **551**, A135 (2013).
22. A. Bhattacharjee, Y.-M. Huang, H. Yang, B. Rogers, *Phys. Plasmas* **16**, 112102 (2009).
23. D. B. Melrose, *Space Sci. Rev.* **26**, 3–38 (1980).
24. E.-H. Kim, I. H. Cairns, P. A. Robinson, *Phys. Plasmas* **15**, 102110 (2008).
25. G. Thejappa, D. Lengyel-Frey, R. G. Stone, M. L. Goldstein, *Astrophys. J.* **416**, 831 (1993).

26. L. Yin, M. Ashour-Abdalla, M. El-Alaoui, J. M. Bosqued, J. L. Bougeret, *Geophys. Res. Lett.* **25**, 2609–2612 (1998).
27. F. Guo, J. Giacalone, *Astrophys. J.* **753**, 28 (2012).
28. G. Li, X. Kong, G. Zank, Y. Chen, *Astrophys. J.* **769**, 22 (2013).
29. E. P. Carley *et al.*, *Nat. Phys.* **9**, 811–816 (2013).
30. D. Burgess, *Astrophys. J.* **653**, 316–324 (2006).

## ACKNOWLEDGMENTS

The authors thank the National Radio Astronomy Observatory (NRAO) staff for their support and E. DeLuca, K. Reeves, H. Tian, J. Lin, A. Warmuth, H. Hudson, A. Caspi, F. Guo, G. Nita, G. Fleishman, and X. Bai for helpful discussions. S. Bourke and G. Hallinan are acknowledged for making their fast radio imaging

software AIPSLITE available for B.C. A. K. Tolbert and R. Schwartz are thanked for their help in providing the Fermi/GBM detector response for this flare. Z. Wang and M. DeRosa are thanked for their help on the Prss extrapolations. The NRAO is a facility of the National Science Foundation (NSF) operated under cooperative agreement by Associated Universities, Inc. The VLA data can be accessed at <https://archive.nrao.edu/archive/advquery.jsp>, using the observing times as the search criteria. The Solar Dynamics Observatory/AIA, RHESSI, Hinode/XRT, and Solar and Heliospheric Observatory/LASCO data are all available through the Virtual Solar Observatory (<http://sdac.virtualsolar.org/cgi/search>). B.C. acknowledges support by NASA under contract SPO2HL701R from Lockheed-Martin to the Smithsonian Astrophysical Observatory (SAO) and contract NNM07AB07C to SAO, and by the NASA Living With a Star Jack Eddy Fellowship (administered by the University Corporation for

Atmospheric Research). C.S.'s work was supported by NSF SHINE grants AGS-1156076 and AGS-1358342 to SAO. D.E.G. acknowledges support from NSF grant AST-1312802 and NASA grant NNX14AK66G to the New Jersey Institute of Technology. S.K. and L.G. are supported by NASA contract NAS598033 for the RHESSI spacecraft.

## SUPPLEMENTARY MATERIALS

[www.sciencemag.org/content/350/6265/1238/suppl/DC1](http://www.sciencemag.org/content/350/6265/1238/suppl/DC1)

Materials and Methods

Figs. S1 to S6

References (31–56)

Movie S1

24 June 2015; accepted 3 November 2015

10.1126/science.aac8467

## BLACK HOLES

# Resolved magnetic-field structure and variability near the event horizon of Sagittarius A\*

Michael D. Johnson,<sup>1\*</sup> Vincent L. Fish,<sup>2</sup> Sheperd S. Doeleman,<sup>1,2</sup> Daniel P. Marrone,<sup>3</sup> Richard L. Plambeck,<sup>4</sup> John F. C. Wardle,<sup>5</sup> Kazunori Akiyama,<sup>2,6,7</sup> Keiichi Asada,<sup>8</sup> Christopher Beaudoin,<sup>2</sup> Lindy Blackburn,<sup>1</sup> Ray Blundell,<sup>1</sup> Geoffrey C. Bower,<sup>9</sup> Christiaan Brinkerink,<sup>10</sup> Avery E. Broderick,<sup>11,12</sup> Roger Cappallo,<sup>2</sup> Andrew A. Chael,<sup>1</sup> Geoffrey B. Crew,<sup>2</sup> Jason Dexter,<sup>13</sup> Matt Dexter,<sup>4</sup> Robert Freund,<sup>2</sup> Per Friberg,<sup>14</sup> Roman Gold,<sup>15</sup> Mark A. Gurwell,<sup>1</sup> Paul T. P. Ho,<sup>8</sup> Mareki Honma,<sup>6,16</sup> Makoto Inoue,<sup>8</sup> Michael Kosowsky,<sup>1,2,5</sup> Thomas P. Krichbaum,<sup>17</sup> James Lamb,<sup>18</sup> Abraham Loeb,<sup>1</sup> Ru-Sen Lu,<sup>2,17</sup> David MacMahon,<sup>4</sup> Jonathan C. McKinney,<sup>15</sup> James M. Moran,<sup>1</sup> Ramesh Narayan,<sup>1</sup> Rurik A. Primiani,<sup>1</sup> Dimitrios Psaltis,<sup>3</sup> Alan E. E. Rogers,<sup>2</sup> Katherine Rosenfeld,<sup>1</sup> Jason SooHoo,<sup>2</sup> Remo P. J. Tilanus,<sup>10,19</sup> Michael Titus,<sup>2</sup> Laura Vertatschitsch,<sup>1</sup> Jonathan Weintraub,<sup>1</sup> Melvyn Wright,<sup>4</sup> Ken H. Young,<sup>1</sup> J. Anton Zensus,<sup>17</sup> Lucy M. Ziurys<sup>3</sup>

Near a black hole, differential rotation of a magnetized accretion disk is thought to produce an instability that amplifies weak magnetic fields, driving accretion and outflow. These magnetic fields would naturally give rise to the observed synchrotron emission in galaxy cores and to the formation of relativistic jets, but no observations to date have been able to resolve the expected horizon-scale magnetic-field structure. We report interferometric observations at 1.3-millimeter wavelength that spatially resolve the linearly polarized emission from the Galactic Center supermassive black hole, Sagittarius A\*. We have found evidence for partially ordered magnetic fields near the event horizon, on scales of ~6 Schwarzschild radii, and we have detected and localized the intrahour variability associated with these fields.

Sagittarius A\* (Sgr A\*) emits most of its  $\sim 10^{36}$  erg/s luminosity at wavelengths just short of 1 mm, resulting in a distinctive “submillimeter bump” in its spectrum (*1*). A diversity of models attribute this emission to synchrotron radiation from a population of relativistic thermal electrons in the innermost accretion flow (*2–4*). Such emission is expected to be strongly linearly polarized, ~70% in the optically thin limit for a highly ordered magnetic field configuration (*5*), with its direction tracing the underlying magnetic field. At 1.3-mm wavelength, models of magnetized accretion flows predict linear polarization fractions  $> \sim 30\%$  (*6–9*), yet connected-element interferometers measure only a 5 to 10% polarization fraction for Sgr A\*

(*10, 11*), which is typical for galaxy cores (*12*). However, the highest resolutions of these instruments, ~0.1 to 1", are insufficient to resolve the millimeter emission region, and linear polarization is not detected from Sgr A\* at the longer wavelengths at which facility very-long-baseline interferometry (VLBI) instruments offer higher resolution (*13*). Thus, these low-polarization fractions could indicate any combination of low intrinsic polarization, depolarization from Faraday rotation or opacity, disordered magnetic fields within the turbulent emitting plasma, or ordered magnetic fields with unresolved structure, leading to a low beam-averaged polarization. The higher polarization seen during some near-infrared flares may support the last possibility (*14, 15*),

but the origin and nature of these flares is poorly understood and may probe a different emitting electron population than is responsible for the energetically dominant submillimeter emission.

To definitively study this environment, we are assembling the Event Horizon Telescope (EHT), a global VLBI array operating at 1.3-mm wavelength. Initial studies with the EHT have spatially resolved the ~40 micro-arc sec emission region of Sgr A\* (*16, 17*), suggesting the potential for polarimetric VLBI with the EHT to resolve its magnetic field structure. For comparison, Sgr A\* has a mass of  $\sim 4.3 \times 10^6 M_{\odot}$  ( $M_{\odot}$ , solar mass) and lies at a distance of ~8 kpc, so its Schwarzschild radius ( $R_{\text{Sch}} = 2GM/c^2$ ) is  $1.3 \times 10^{12}$  cm and subtends 10 micro-arc sec (*18, 19*). In March 2013, the EHT observed Sgr A\* for five nights using sites in California, Arizona, and Hawaii. In California, we phased together eight antennas from the

<sup>1</sup>Harvard-Smithsonian Center for Astrophysics, 60 Garden Street, Cambridge, MA 02138, USA. <sup>2</sup>Haystack Observatory, Route 40, Massachusetts Institute of Technology, Westford, MA 01886, USA. <sup>3</sup>Steward Observatory, University of Arizona, 933 North Cherry Avenue, Tucson, AZ 85721-0065, USA. <sup>4</sup>Department of Astronomy, Radio Astronomy Laboratory, 501 Campbell, University of California Berkeley, Berkeley, CA 94720-3411, USA. <sup>5</sup>Department of Physics MS-057, Brandeis University, Waltham, MA 02454-0911. <sup>6</sup>National Astronomical Observatory of Japan, Osawa 2-21-1, Mitaka, Tokyo 181-8588, Japan. <sup>7</sup>Department of Astronomy, Graduate School of Science, The University of Tokyo, 7-3-1 Hongo, Bunkyo-ku, Tokyo 113-0033, Japan. <sup>8</sup>Institute of Astronomy and Astrophysics, Academia Sinica, Post Office Box 23-141, Taipei 10617, Taiwan. <sup>9</sup>Academia Sinica Institute for Astronomy and Astrophysics (ASIAA), 645 N. A'ohōkū Pl. Hilo, HI 96720, USA. <sup>10</sup>Department of Astrophysics/Institute for Mathematics, Astrophysics and Particle Physics, Radboud University Nijmegen, Post Office Box 9010, 6500 GL Nijmegen, Netherlands. <sup>11</sup>Perimeter Institute for Theoretical Physics, 31 Caroline Street North, Waterloo, ON N2L 2Y5, Canada. <sup>12</sup>Department of Physics and Astronomy, University of Waterloo, 200 University Avenue West, Waterloo, ON N2L 3G1, Canada. <sup>13</sup>Max Planck Institute for Extraterrestrial Physics, Giessenbachstrasse 1, 85748 Garching, Germany. <sup>14</sup>James Clerk Maxwell Telescope, East Asia Observatory, 660 N. A'ohōkū Place, University Park, Hilo, HI 96720, USA. <sup>15</sup>Department of Physics, Joint Space-Science Institute, University of Maryland at College Park, Physical Sciences Complex, College Park, MD 20742, USA. <sup>16</sup>Graduate University for Advanced Studies, Mitaka, 2-21-1 Osawa, Mitaka, Tokyo 181-8588. <sup>17</sup>Max-Planck-Institut für Radioastronomie, Auf dem Hügel 69, D-53121 Bonn, Germany. <sup>18</sup>Owens Valley Radio Observatory, California Institute of Technology, 100 Leighton Lane, Big Pine, CA 93513-0968, USA. <sup>19</sup>Leiden Observatory, Leiden University, Post Office Box 9513, 2300 RA Leiden, Netherlands.

\*Corresponding author. E-mail: mjohnson@cfa.harvard.edu



## Particle acceleration by a solar flare termination shock

Bin Chen *et al.*

*Science* **350**, 1238 (2015);

DOI: 10.1126/science.aac8467

*This copy is for your personal, non-commercial use only.*

If you wish to distribute this article to others, you can order high-quality copies for your colleagues, clients, or customers by [clicking here](#).

Permission to republish or repurpose articles or portions of articles can be obtained by following the guidelines [here](#).

**The following resources related to this article are available online at [www.sciencemag.org](http://www.sciencemag.org) (this information is current as of December 6, 2015):**

**Updated information and services**, including high-resolution figures, can be found in the online version of this article at:

<http://www.sciencemag.org/content/350/6265/1238.full.html>

**Supporting Online Material** can be found at:

<http://www.sciencemag.org/content/suppl/2015/12/02/350.6265.1238.DC1.html>

This article **cites 52 articles**, 1 of which can be accessed free:

<http://www.sciencemag.org/content/350/6265/1238.full.html#ref-list-1>

This article appears in the following **subject collections**:

Astronomy

<http://www.sciencemag.org/cgi/collection/astronomy>

Planetary Science

[http://www.sciencemag.org/cgi/collection/planet\\_sci](http://www.sciencemag.org/cgi/collection/planet_sci)